1 Revised, 11/XX/2022

Corrugation-induced active sites on pristine graphene for H₂ activation

3 Qiang Wan,[†] Hua Guo,[‡] and Sen Lin^{*,†}

[†]State Key Laboratory of Photocatalysis on Energy and Environment, College of

Chemistry, Fuzhou University, Fuzhou 350002, China

[‡] Department of Chemistry and Chemical Biology, University of New Mexico,

Albuquerque, New Mexico, 87131, USA

* Corresponding author: slin@fzu.edu.cn

10 Abstract

Pristine graphene is widely considered to be chemically inert, but recent experimental studies have suggested that it can provide frustrated Lewis pairs (FLPs) for activating H₂ under mild conditions. Using density functional theory (DFT) and *ab initio* molecular dynamics (AIMD) calculations, we explore in this work the possibility that corrugation in pristine graphene is responsible for the formation of FLPs and thus its observed catalytic activity. Our DFT results demonstrate that the ease of H₂ activation is proportional to the degree of corrugation of graphene. For corrugated graphene, the two catalytic *para*-carbon sites show clear sign of transient Lewis acid/base properties along the reaction coordinate, a pre-requisite for FLPs. Furthermore, the two dissociating H atoms carry opposite charges, suggesting heterolytic activation of H₂. This behavior is confirmed by AIMD simulations at room temperature, which show that fluctuations of the corrugated graphene lead to C sites

with diverse distances and varying charges. These observations offer a plausible rationalization of the experimental observations and possible design principles for FLP catalysts using homogenous two-dimensional materials.

KEYWORDS: Graphene; corrugation; H₂ activation; hydrogenation; dynamics; frustrated Lewis pairs

1. Introduction

Two-dimensional (2D) graphene (Gr) has attracted significant interest in many fields due to its unique properties compared to bulk-phase materials. ¹⁻² However, unlike bent carbon nanotubes with misaligned orbitals, defect-free Gr has traditionally been considered chemically inert for catalytic reactions due to its uniform sp^2 carbon atoms and delocalized π -electrons in the basal plane. A common approach to endow pristine Gr with catalytic activity is to introduce exotic active sites, such as supporting metals and surface-functionalized doping. ³⁻⁵ Although there have been extensive investigations of the active sites of such modified Gr, little attention has been paid to pristine graphene itself as a catalyst.

In 2014, Primo *et al.* reported for the first time that pristine Gr possesses catalytic activity for hydrogenation of unsaturated hydrocarbons comparable to, or even better than, commercial Pd/C, Pt/C and new Ni/C catalysts.⁶ On the other hand, N/P/S doping of Gr was found to significantly reduce the overall activity, in sharp contrast to previous reports of Gr catalysis through doping.⁷⁻⁸ A key finding of that study is the isotopic H/D scrambling in thermal programmed desorption (TPD) after dosing with H₂ and D₂,

indicating the crucial H₂ (D₂) dissociation for subsequent hydrogenation catalysis. More interestingly, the overall catalytic performance of Gr can be reversibly affected by the addition of CO₂ (a Lewis acid)/NH₃ (a Lewis base) to the reaction stream. It was argued that the NH₃ and CO₂ molecules can reversibly adsorb onto the Gr surface, implying that some carbon species of Gr may exist as Lewis acids and bases, which are neutralized by the external ones. Based on these observations, these authors hypothesized that this unexpected activity of Gr is attributable to the presence of frustrated Lewis pairs (FLPs) on its surface, although the exact mechanism remains unknown.

Catalysis by FLPs is a new and vibrant field.⁹⁻¹¹ The basic premise is that a sterically hindered Lewis acid and base pair can provide an active site that polarizes a molecule such as H₂, leading to its dissociation and formation of protonic and hydridic species.¹²⁻¹³ This FLP mechanism, originally suggested in homogeneous catalysis,¹³ has recently found numerous applications in heterogeneous catalysis.¹⁴⁻¹⁶ Since an FLP typically consists of an electron rich and an electron poor species,¹⁷⁻¹⁸ it is not immediately clear how Gr can provide FLPs.

It is well known that the conformation of a material strongly influences its electronic structure, which controls its physical and chemical properties.¹⁹ Since the discovery of Gr, the intrinsic properties of pristine Gr have been hotly debated because different synthesis techniques lead to different morphological features (e.g., number of layers, degree of smoothness, and defect concentration), making it a serious challenge to establish a unified structure-activity relationship.²⁰⁻²³ A growing number of studies

has shown that the presence of deformation of the planar Gr can directly influence its electronic structure, ²⁴⁻²⁷ leading to a variety of applications. ²⁸⁻³⁰ For example, Hu *et al*. reported that wrinkles in exfoliated Gr monolayer can break the 6-fold symmetry of ideal lattice and affect its electrical conductance. 31 Kundalwal et al. demonstrated using density functional theory (DFT) that the symmetry of the π -orbital of pristine Gr can be broken by bending.³² Following this finding, Duggen et al. developed a mathematical model of polarization dynamics of bent Gr and demonstrated the piezoelectric effect, which originates from a dynamically generated surface charge density proportional to the local curvature of the Gr layer.³³ More recently, Huang et al. reported that the chemical reactivity of carbon atoms in wrinkled multilayer Gr is much higher than that in flat regions, as seen from hydrogen plasma etching results.³⁴ This is understandable as the prevalence of corrugations in pristine Gr transforms the isotropic carbon sites to acquire different physicochemical properties. These studies have clearly pointed out the non-negligible influence of corrugation on mechanical and chemical properties of pristine Gr, enabling various applications.

68

69

70

71

72

73

74

75

76

77

78

79

80

81

82

83

84

85

86

87

88

89

Under realistic conditions, it is almost impossible for defect-free Gr to remain completely flat.³⁵ Indeed, we note that in Ref. 6, the TEM images of the Gr used in catalyzing hydrogenation of acetylene have extensive nonplanarity and wrinkles. As discussed above, the effects of corrugation on catalysis should be investigated. In this work, we explore the possibility of FLP formation on corrugated Gr and its role in activating H₂ in hydrogenation catalysis. To this end, we constructed a series of corrugated Gr models and studied their catalytic activity by DFT and *ab initio*

molecular dynamics (AIMD) calculations in relation to planar Gr.

90

91

92

93

94

95

96

97

98

99

100

101

102

103

104

105

106

107

108

109

110

111

Our investigation starts with an ideal planar Gr monolayer adopted to represent the flat region of the pristine Gr and its properties were investigated as the reference. This is followed by the investigation of corrugated Gr models. Our results clearly show that the H₂ dissociation barrier has a negative correlation with the degree of corrugation in Gr, revealing its catalytic potential. Further investigations of the entire acetylene hydrogenation process revealed that the activation of H₂ is the rate-determining step while the subsequent hydrogenation catalysis is facile. More importantly, charge distributions in the catalytic site show clear signs of a transient FLP formation along the reaction coordinate. This is supported by AIMD simulations at finite temperatures which revealed unique dynamical behaviors of the catalytic C sites on corrugated Gr, particularly the formation of different C-C distances and various charge states, underscoring different electron gain/loss abilities of the C sites as the system approaches the transition state (TS). Such a transient FLP polarizes H₂, leading to the formation of protonic and hydridic species. These observations substantiate the FLP hypothesis of Primo *et al.* in Gr catalyzed hydrogenation of unsaturated hydrocarbons and offer insights into the catalytic potential of this seemingly inert material.

2. Computational Details

All spin-polarized DFT calculations were carried out by using the Vienna *Ab initio* Simulation Package (VASP).³⁶ The exchange-correlation functional was described by the Perdew-Burke-Ernzerhof (PBE) functional within the generalized gradient approximation (GGA),³⁷⁻³⁸ while the core electrons were described by the projector-

augmented wave (PAW) method.³⁹ The wave functions of valance electrons were expanded in plane waves with cut-off energy of 400 eV. A correction of the van der Waals dispersion was considered with the DFT-D2 method of Grimme.⁴⁰

112

113

114

115

116

117

118

119

120

121

122

123

124

125

126

127

128

129

130

131

132

133

A periodic orthorhombic $3\sqrt{3} \times 4$ supercell of Gr monolayer consisting of 48 C atoms was used to model the Gr. A k-mesh of $3 \times 3 \times 1$ was adopted to sample the Brillouin zone, which was tested to be converged. The separation between different images of the periodic slab in the z-direction was kept at 15 Å to avoid the interaction between periodic slabs. The lengths of lattice vectors of the xy plane of ideal Gr (a₀ and b_0) are 12.78 and 9.84 Å. To simulate corrugated Gr, we have followed a commonly used procedure in which the unit cell lengths are scaled. Specifically, a scaling factor (s $= a/a_0 = b/b_0$) was applied to the lattice vectors a and b. In order to release the strain in the model, all the structures underwent NVT equilibration (2 ps) at 300 K before carrying out further calculations. Snapshots were taken near the end of the equilibration trajectories and the corresponding structures are relaxed by minimizing the total energy, with convergence criteria for energy and force set to 10⁻⁴ eV and 0.02 eV/Å, respectively. The atomic charge was calculated based on Bader charge analysis,⁴¹ although other schemes (e.g., Mulliken) have been tried and yield qualitatively the same results. The definition and calculation details related to the Fukui function are presented in S1 of the Supporting Information (SI).

The climbing image-nudged elastic band (CI-NEB) 42 method and the dimer method 43 were used to determine TSs of H₂ activation and acetylene hydrogenation. In this case, the convergence criteria for energy and force were set to 10^{-7} eV and 0.02

eV/Å, respectively. Meanwhile, the slow-growth (SG) approach⁴⁴ was used to shed light on the dynamic behaviors of Gr and H_2 , as the system approaches the TS of H_2 dissociation along a collective variable (CV) that defines the reaction coordinate. Details can be seen in S2 of SI (Figure S1-S3 and Table S1).

3. Results

3.1 Flat graphene

Due to the sp^2 hybridization characteristics of carbon atoms, defect-free Gr exhibits a hexagonal honeycomb structure, which is usually modeled as a completely planar layer. Here, we first performed a 2 ps NVT simulation at room temperature to examine the structural fluctuations and the results are shown in Figure 1a. For flat Gr, we found that the structural deformation was very slight, as evidenced by the relatively small fluctuations in Gr thickness, which is defined as the height difference between the highest atom and the lowest atom in the z-direction, in the range of 0.24 to 0.75 Å.

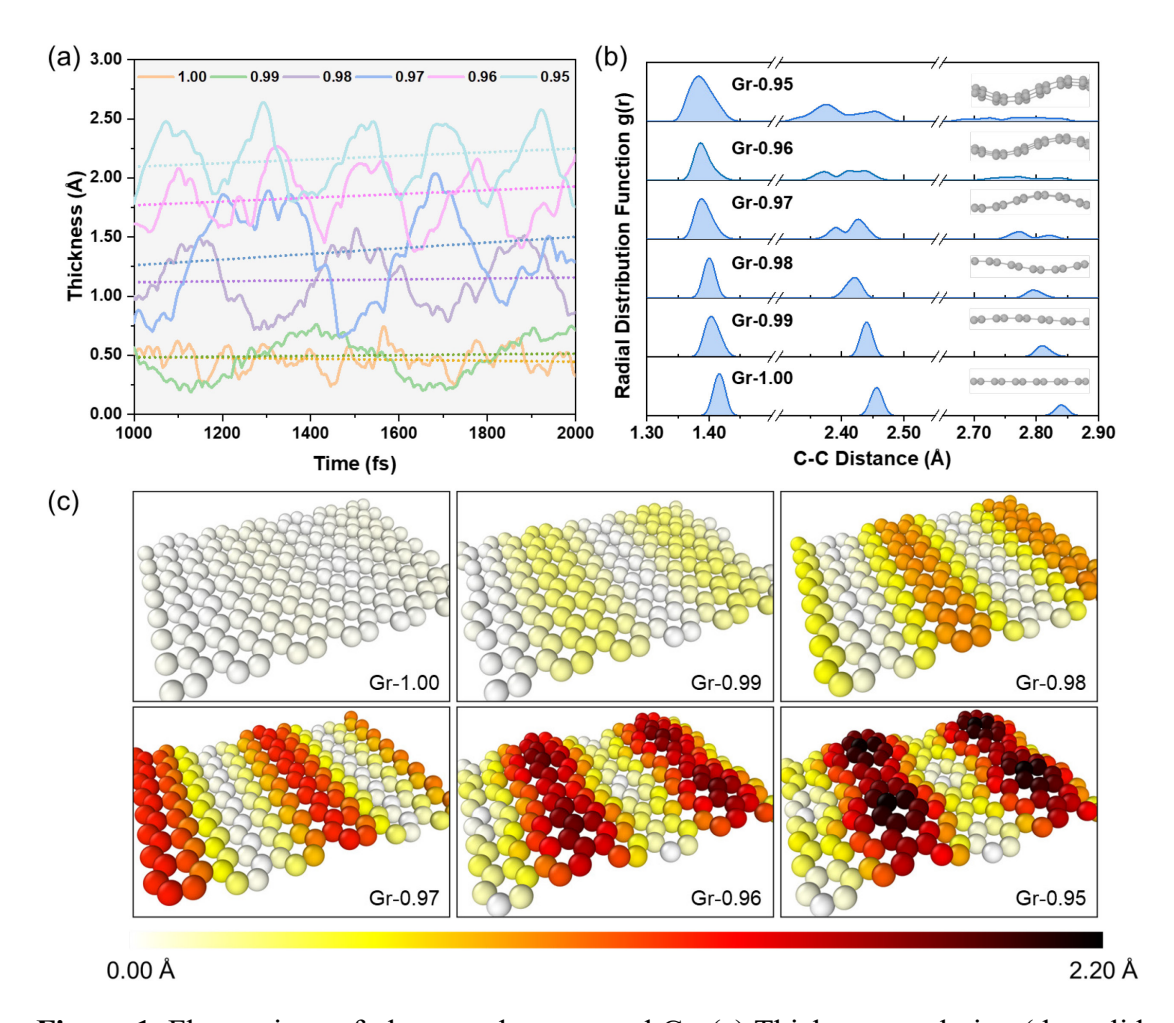


Figure 1. Fluctuations of planar and corrugated Gr. (a) Thickness evolution (the solid lines) in the last 1 ps after the system reached equilibrium of NVT equilibration and average thickness (dashed lines). (b) Radial distribution functions of C-C pairs in optimized corrugated Gr after the NVT equilibration. (c) Sample structures of 2×2 optimized Gr-s (s = 1.00 to 0.95) after the NVT simulation, colored according to z-coordinates (heights) of atoms.

Subsequently, we investigated the capacity of flat Gr for H₂ activation at different sites. Two C sites in the same six-membered ring on defect-free Gr are required for H₂ dissociation. Three C-C site combinations were considered (Figure 2a), *i.e.*, *ortho*-C-C, *meta*-C-C and *para*-C-C, with the corresponding C-C distances of 1.42, 2.46, and 2.84

Å, respectively. The H₂ dissociation barriers at these three C-C combinations are shown in Figure 2b. It can be seen that the H₂ dissociation has the lowest barrier of 2.88 eV at the *para*-C-C site, while the other two C-C sites have higher barriers (up to 3.73 eV). Structurally, the C active sites in the TS and final state (FS) at the *para*-site are slightly pulled up by the H species, due apparently to their conversion from sp^2 to sp^3 hybridization. The inflexibility of the active sites (see Figure 1a) due to planarity enforced by the delocalized π bonds is likely responsible for the high energy barrier. Clearly, such large energy barriers render the direct catalytic dissociation of hydrogen on flat Gr very difficult if not impossible, especially at the temperature reported by Primo *et al.* (~120 °C).⁶ These results are also consistent with the conventional wisdom that pristine Gr is chemically inert.

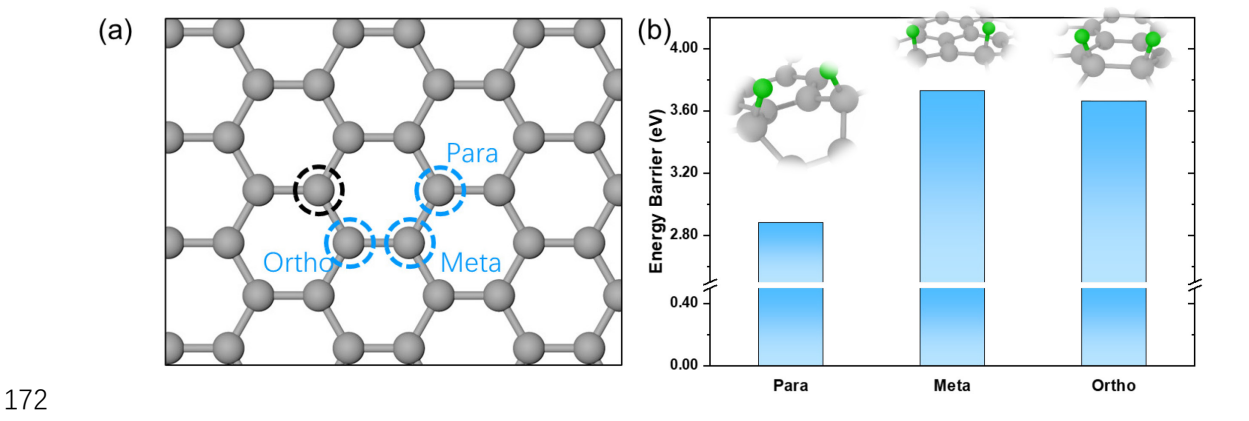


Figure 2. H₂ dissociation on planar Gr. (a) Different catalytic sites on Gr consisting of an arbitrary carbon represented by the black dash circle and blue dash circle of a nearby carbon site denoted as *para*, *meta*, or *ortho* carbon. (b) The corresponding energy barriers and FS structures. Color code: grey, carbon; green, hydrogen.

3.2 Corrugated graphene

3.2.1 Models

178

179

180

181

182

183

184

185

186

187

188

189

190

191

192

193

194

195

196

197

198

199

As discussed above, flat Gr has negligible structural deformation and thus limited ability for catalyzing dissociation of H₂. It is thus natural to ask the question of whether the more pronounced deformation in synthesized Gr, which have been widely reported in the literature, 35 may lead to catalytic activity. Such deformation could potentially provide sites with unconventional properties, which might lower the barrier of H₂ activation. To answer this question, we use a common method for constructing surface corrugations in both experiments and theoretical simulations, namely by applying an external strain to the basal plane. ^{28, 47-49} In our models, a scaling factor ($s = a/a_0 = b/b_0$) was introduced to describe the degree of lattice contraction. After applying s to lattice vectors, a 2 ps NVT equilibration was carried out for each model to sample the configuration space. In the NVT simulation, significant out-of-plane vibrations of the constituent carbon atoms were observed. Finally, corrugations were formed with the C-C bond lengths ranging from 1.35 to 1.45 Å, in good agreement with the experimentally reported average value of 1.41 Å for a monolayer Gr. 50 The resulting Gr monolayers with different degrees of corrugation are denoted as Gr-s (s is the scaling factor). Figure 1a shows the thickness variation of several Gr-s models in the last 1 ps of simulation, in comparison with that of the planar Gr (Gr-1.00). Comparing to Gr-1.00, the fluctuation becomes substantially more pronounced when the s value is reduced to 0.98 and 0.95. Indeed, the average thickness of Gr in the last 1 ps simulation is negatively correlated with the s value, as discussed below.

After the NVT simulations, all structures were subjected to energy minimization for the subsequent analysis. The C-C distance distribution of the optimized Gr-s is shown in Figure 1b, where it can be seen that the range of the C-C distance distribution at the *para*-sites (\sim 2.80 Å) becomes wider as the Gr corrugation increases with decreasing s, demonstrating the structural diversity of the potential active sites on corrugated Gr. The trend can be clearly seen from the optimized structures that shown in Figure 1c. The relationship among s, Gr-s thickness, and catalytic activity is analyzed in the next section.

Next, we examine the electronic structures of Gr-1.00 (Figure S4) and Gr-0.95 (Figure 3a-b and Figure S5) as examples. Interestingly, as shown in Figure S4a, the charges of all C atoms on Gr-1.00 are almost equal to zero, as expected. However, C atoms on Gr-0.95 show significant charge differences (Figure 3a), suggesting that charges are no longer uniformly and symmetrically distributed on the constituting C atoms in the corrugated Gr. Indeed, some of the C atoms are positively charged, while others are negatively charged. Correspondingly, the Fukui functions $f^{+/-}(\mathbf{r})$ for Gr-1.00 show good symmetry (Figure S4b), while those in Gr-0.95 are apparently asymmetric (Figure 3b), implying that corrugation promotes diversity in the electronic structure and charge distribution at surface C sites. Also, as can be seen in Figure 3b, the profiles of $\Delta f(\mathbf{r})$ show different shapes around the Gr-0.95 surface, suggesting different electron affinity of C atoms, which can be contrasted to near uniform $\Delta f(\mathbf{r})$ on Gr-1.00 (Figure S2b). Globally, the differing nucleophilicity and electrophilicity are clearly seen from the fluctuating atomic condensed dual descriptor in Gr-0.95 (Figure

S5), which is in sharp contrast to the nearly equal ones on Gr-1.00 (Figure S4c). These observations strongly suggest that carbon atoms on corrugated Gr have increased electron gain/loss capabilities, which could potentially provide FLP sites for H₂ activation.

3.2.2 Catalytic activity

In this section, the catalytic performance of a series of Gr-s models is investigated. We first focus on the hydrogen adsorption and dissociation on the Gr-0.95 surface, as shown in Figure 3c and Figure S1. The most stable adsorption state of H₂ on Gr-0.95 is used as the IS for the CI-NEB calculation. The results show that the TS, featuring an elongated H–H bond and two puckered-up carbons, yields an energy barrier of 1.74 eV, which is significantly lower than that on pristine Gr as discussed above (2.88 eV). In the FS, the two dissociated hydrogens adsorb on *para*-C-C sites, respectively, forming two C–H species. Structure b is further converted to lower energy structure c without a barrier. The much lower dissociation barrier for H₂ on Gr-0.95 than the flat Gr suggests that the corrugation helps to promote the catalysis.

To gain insight into the origin of the catalytic activity, we have plotted the charges of the two carbon atoms at the active site and the hydrogen atoms for several CI-NEB images. As mentioned above, the two carbon atoms at the active site have opposite charges, but both become negatively charged after H₂ adsorption (IS). As shown in Figure 3d, they regain opposite signs in some CI-NEB images between the IS and TS, suggesting the emergence of a sterically frustrated Lewis acid-base pair. This is accompanied by the opposite charges in the two hydrogens, implying that the H₂

activation followed a heterolytic mechanism and led to protonic and hydridic species. Interestingly, the final charges of the H species at the TS become positive, apparently dictated by the difference between the electronegativity of H and C. Nonetheless, the transient protonic and hydridic characters strongly suggest that the H₂ is polarized by the transient FLP provided at the *para*-site. This ability to form a transient FLP can be attributed to the ability of the C active sites to gain/loss electrons facilitated by the corrugation and the flexible C-C distances during dynamics.

We have repeated the CI-NEB calculation for H₂ dissociation on corrugated Gr with several scaling factors. As shown in Figure 3e, the barrier is positively correlated with the scaling factor, which is negatively correlated with the thickness of the Gr. In other words, the larger the strain in the Gr, the thicker it becomes, and the lower the activation barrier. Specifically, the energy barrier of H₂ activation decreases significantly from 2.88 eV at Gr-1.00 to 1.74 eV at Gr-0.95. (See Table S2 for energy barriers and imaginary frequencies for other *s* values in between.) It is worth noting from the TS configurations shown in Figure S6 that the smaller *s* values, which correspond to larger corrugation, results in shorter C-C distance of the *para*-active site.

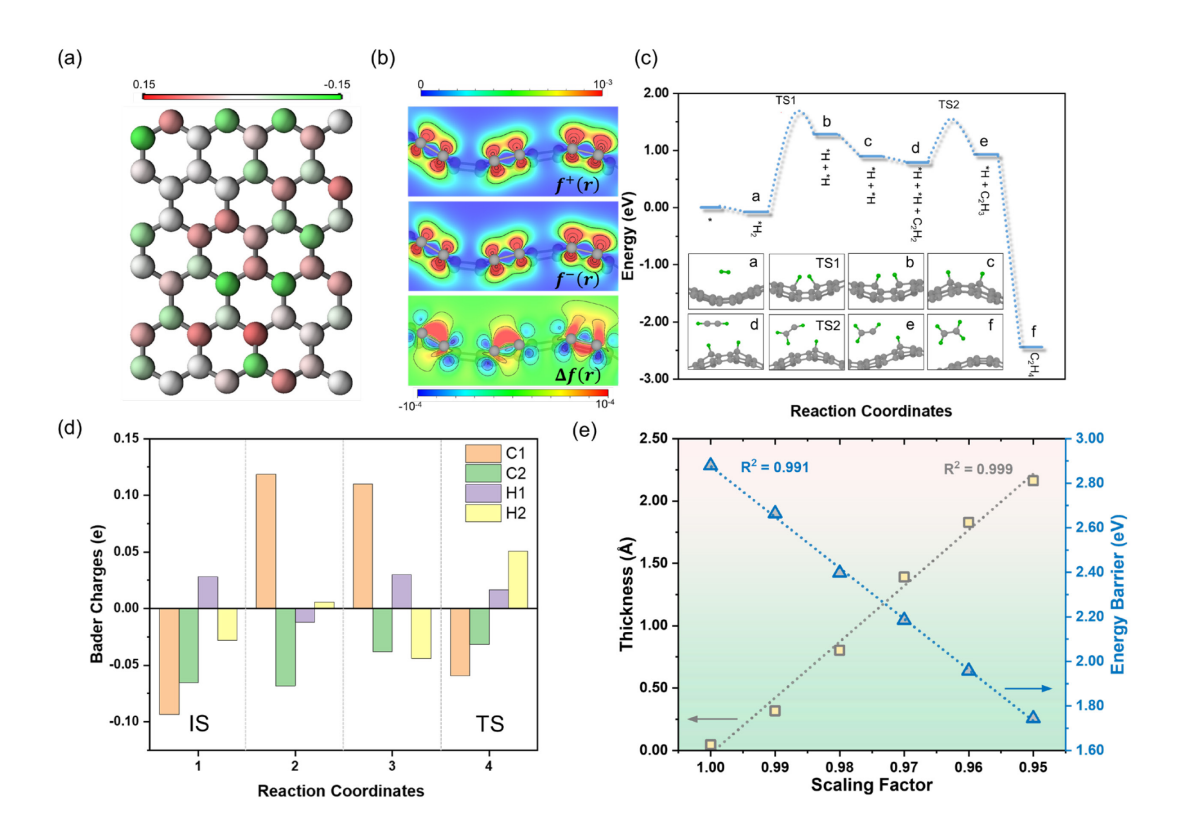


Figure 3. Electronic and catalytic properties of corrugated Gr. (a) Charge distribution in Gr-0.95 (top view), in which the charge is color coded with the scale on top. (b) Cross-sectional profiles of $f^+(\mathbf{r})$, $f^-(\mathbf{r})$ and $\Delta f(\mathbf{r})$ of Gr-0.95 (side view) in e/Bohr³. (c) Energy profile of acetylene hydrogenation catalyzed by Gr-0.95. Color Scheme: C, grey; H, green. (d) Bader charge evolution of the *para*-sites (C1, C2) and two H (H1, H2) from the IS to TS in H2 dissociation on Gr-0.95. 1 and 4 in reaction coordinates correspond to the IS and TS, respectively, while 2 and 3 correspond to the activated H–H species between IS and TS. Detailed CI-NEB energy profile with structures were shown in Figure S1. (e) Correlation between the thickness of corrugated Gr with the scaling factor and with the corresponding energy barrier for H2 activation.

We have further reduced the scaling factor from 0.94 to 0.88, but for s < 0.94, the trend of increasing thickness starts to slow down and the difference between those at s

= 0.91 and s = 0.90 is merely 0.025 Å, as shown in Figure S7a. However, the energy barrier for hydrogen activation drops to 1.35 eV at s = 0.92. As s continues to drop, the energy barrier fluctuates around 1.40 eV, see Figure S7b. (Gr models with even smaller s were not considered for H₂ activation due to severe deformation of these surfaces, as shown in Figure S8.) These results provided further evidence that Gr corrugation plays an important role in promoting catalytic H₂ activation.

We also studied the acetylene hydrogenation by the H* species formed from H_2 dissociation ($C_2H_2*+2H*\to C_2H_4*$). Taking Gr-0.95 as an example (Figure 3c), C_2H_2* is found to physisorb on the Gr surface with an adsorption energy of -0.11 eV. In the first hydrogenation step, it reacts with a nearby hydrogen atom to form the C_2H_3* intermediate ($C_2H_2*+H*\to C_2H_3$), which has an energy barrier of 0.74 eV. In the second step, the C_2H_3 intermediate is spontaneously hydrogenated to C_2H_4* with no energy barrier. The C_2H_4 product has a small adsorption energy of -0.13 eV, which can be expected to desorb readily from the catalyst surface. The barrier for hydrogenation is much lower than H_2 dissociation, making the latter rate limiting. The further hydrogenation of C_2H_4 by surface H has an energy barrier of 0.74 eV (Figure S9), which is difficult to compete with desorption. In addition, the acetylene hydrogenation catalyzed by Gr-1.00 have also been investigated (Figure S10). In this case, the hydrogenation takes place following the same mechanism with that over Gr-0.95 and the barrier is 0.60 eV. As a result, the H_2 activation remains the rate-determining step.

To be complete, the catalytic performance of Gr edge sites such as armchair and zigzag edges were also explored. It was found from Figure S11 that the H₂ dissociation

at these edge sites has either an extremely small (0.06 eV) or null barrier, with energy releases of -5.34 and -5.43 eV, respectively, due to the strong binding of H to unsaturated C. However, the overly strong chemisorption of H species at C sites results in extreme endothermicity for the hydrogenation of acetylene at these defective sites (2.98 eV for armchair sites and 3.03 eV for zigzag sites, Figure S12). These results effectively rule out edge sites as the active sites for hydrogenation, confirming the argument made by Primo *et al.*⁶ The above results suggest that defect-free but corrugated Gr is more likely to provide the relevant active sites for the hydrogenation catalysis.

3.2 Impact of dynamics on catalysis

Since the morphology of Gr monolayers is constantly changing during the catalysis, studying the reaction process based only on static DFT calculations may not be sufficient to understand the dynamic behaviors in the catalysis.

In this section, we discuss AIMD simulations of the H₂ dissociation at 300 K with the slow-growth (SG) approach, ⁵¹ using Gr-1.00 and Gr-0.95 as examples. In the SG approach, the IS is slowly switched to the TS along a collective variable (CV). The fluctuation of various properties is followed along the trajectory, which sheds light on the dynamics. As shown in Figure 4a, during the H₂ activation catalyzed by Gr-1.00, the distance of *para*-C-C fluctuates and decreases from 2.82 to 2.69 Å until it reaches the TS, marked in the figure by the vertical gray line, while the H–H distance increases to 1.27 Å. However, as displayed in Figure 4b, for Gr-0.95, the initial C–C distance (2.76 Å) is slightly shorter than that (2.82 Å) of Gr-1.00, but decreases more rapidly to

2.50 Å at the TS, with a corresponding distance between H–H of 1.00 Å. In other words, compared with Gr-1.0, a Gr with larger corrugation (Gr-0.95) is more likely to generate a shorter *para*-C-C distance, which leads to a stronger interaction between the elongated H–H and Gr, thus reducing the energy barrier of H₂ cleavage.

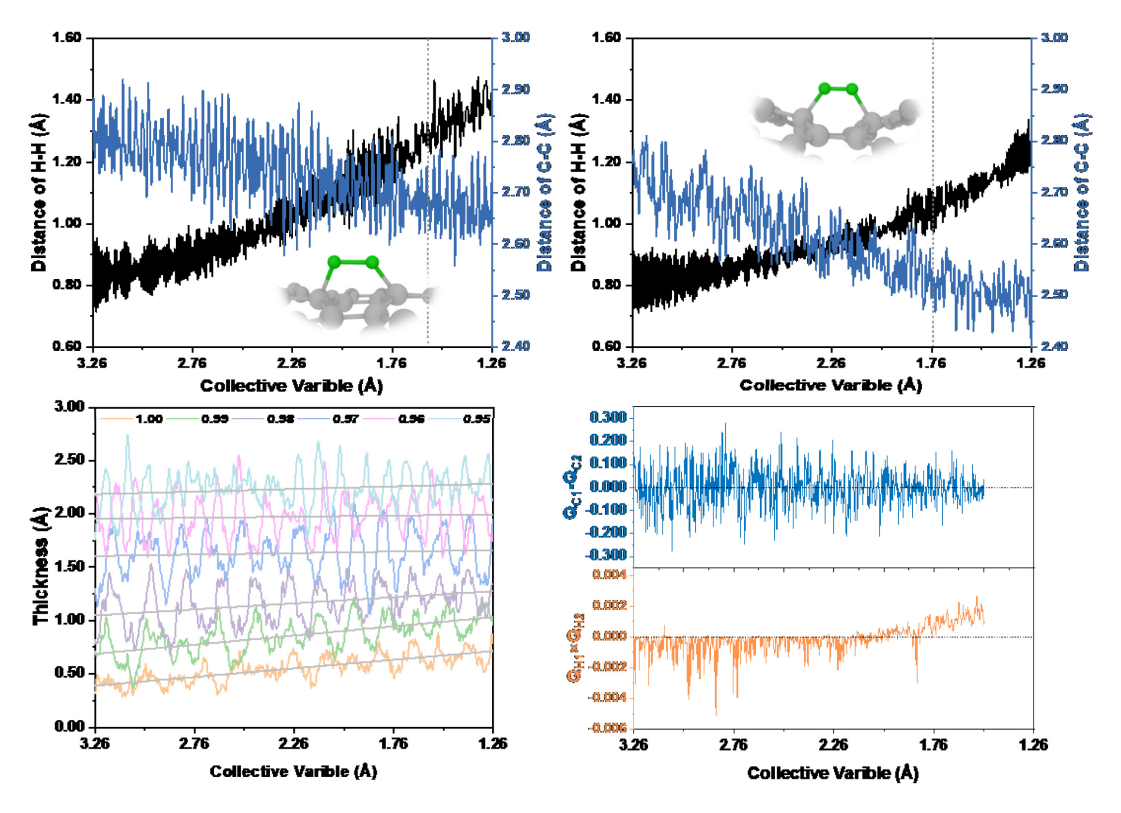


Figure 4. Dynamics along the reaction coordinate. Evolution of the H–H and C–C distances along the CV for H₂ dissociation catalyzed by (a) Gr-1.00 and (b) Gr-0.95, the highest point of the free energy (the TS) was labeled by grey dash line. Color scheme: C, grey; H, green. (c) Thickness evolution of Gr (s from 0.95 to 1.00) during H₂ dissociation. (d) Charge difference (Q_{C1} - Q_{C2}) between Q_{C1} and Q_{C2} and charge product ($Q_{H1} \times Q_{H2}$) of Q_{H1} and Q_{H2} in the process of H₂ dissociation catalyzed by Gr-0.95. The negative value of $Q_{H1} \times Q_{H2}$ means that the charge states of the two H species are opposite, while the positive value represents the same charge state.

In Figure 1a-b, we find that the larger thicknesses allow the C-C distance of Gr-s to fluctuate over a larger range in the absence of H₂. Herein, the thickness of a series of Gr-s was investigated during H₂ activation. As shown in Figure 4c, the thickness of Gr-1.00, 0.99 and 0.98 show obvious increasing trends as the H₂ is activated, and for the other three corrugated Gr (Gr-0.97, 0.96 and 0.95), which possess larger thickness, the trends are much weaker. This implies that the thickness of the less corrugated Gr varies more than that of highly corrugated Gr. Considering that the *para*-C-C distance decreases when H₂ dissociates (Figure 4a-b), we regarded it as a reasonable phenomenon that the more corrugated Gr has more flexible C active sites and therefore the catalyst surface does not need much deformation, which requires extra energy, to catalyze the activation of H₂.

In addition to the dynamical structural features discussed above, the analysis of charge changes in the activation is essential for a deeper understanding of the mechanism. To test the FLP hypothesis of Primo *et al.*, we analyzed the fluctuation of the charge (Q) of the two C atoms and two H atoms during H₂ activation, as depicted in Figure 4d (upper panel). It is clear from the figure that the two carbons have significant transient charge differences (Q_{C1} - Q_{C2}). This charge imbalance signifies that the two C atoms could provide the FLP on a transient basis, which can polarize the H₂ and help its bond cleavage. Indeed, in Figure 4d (lower panel), the product of the H charges $Q_{H1} \times Q_{H2}$ clearly shows transient protonic and hydridic characters, leading to the TS, consistent with the CI-NEB results shown in Figure 3.

4. Discussion and Conclusions

Gr materials consisting of sp^2 C atoms are traditionally considered to be inert to H₂ activation. Numerous efforts have been made to introduce new active sites (e.g., noble metal doping) in Gr to catalyze reactions. We in this work are concerned with the recent discovery by Primo *et al.*, 6 who reported the surprising reactivity of pristine Gr in acetylene hydrogenation. Despite strong circumstantial evidence presented by these authors, however, it was unclear what are the mechanism and factors affecting the reactivity. Our premise in this work is that the surface morphology of Gr is not always planar under realistic conditions, including the experiment by Primo *et al.* Indeed, corrugations could exist under many practical conditions, such as different synthesis temperatures and pressures. Such surface corrugations could conceivably lead to catalytic sites. This hypothesis has so far attracted little attention.

In this current work, we constructed several Gr monolayers with different degrees of corrugation to investigate H₂ activation using static and dynamical methods. The DFT results show that the introduction of corrugations can indeed significantly reduce the energy barrier for H₂ activation compared to flat Gr. Indeed, the degree of corrugations correlates well with the energy barrier. The origin of this correlation derives from the fact that the presence of corrugations generates surface C-C sites with diverse structure fluctuations, which alter the electronic properties. These active sites possess significant charge fluctuations, which can efficiently polarize the H₂ molecule to form active surface H species for the subsequent hydrogenation steps, very similar to the mechanism of FLP catalysis. Our results suggest that the activation of H₂, a rate-

determining step in acetylene hydrogenation, can be effectively regulated by controlling its surface morphology without the introduction of any exotic active site.

We stress that the catalysis discussed in this work is difficult to be classified as an FLP in the conventional sense, because the two carbon atoms in the catalytic *para*-site do not possess opposite charges before hydrogen binding. Rather, a sterically hindered Lewis acid-base pair emerges *transiently* during the H₂ activation. Fontaine and Stephan have extensively discussed the non-conventional definition of FLP chemistry, in which the FLP does not have to be a pre-existing condition. The case discussed here seems to be such a case and can probably be best described as a transient FLP. Nonetheless, the catalytic effect is quite apparent, evidenced by the drastic reduction of the reaction barrier.

Admittedly, the theory-experiment comparison is not as quantitative as one would wish. Despite the clear demonstration of significant lowering of the barrier by Gr corrugation in this work, the calculated barrier for H₂ dissociation is still quite high. This could presumably be due to various uncertainties in our model, such as the DFT functional used in the calculation and nuclear quantum effects. Indeed, the overcome of the H₂ dissociation barrier might involve significant tunneling, which further reduces the activation energy. Nonetheless, the qualitative conclusions reached by our investigation are robust and offer a unique perspective on how to manipulate structure of materials to create chemical reactivity.

The insights gained in this work enrich our understanding of the potential capacity of 2D materials, including but not limited to Gr monolayers, as catalysts. The present

- 398 work also provides a new perspective to understand FLPs, i.e., asymmetric sites
- 399 composed of the same elements can form FLPs to activate small molecules, further
- 400 expanding the scope of applications in the field of FLP catalysis.

- 402 Acknowledgements: Funds from the National Natural Science Foundation of
- 403 China (21973013 to S.L.) and the National Natural Science Foundation of Fujian
- 404 Province, China (2020J02025 to S.L.) are acknowledged. S.L. thanks the "Chuying
- 405 Program" for the Top Young Talents of Fujian Province. This project is partially funded
- by the U.S. National Science Foundation (CHE-1951328 to H.G.). Computations were
- 407 performed at the Hefei Advanced Computing Center and Supercomputing Center of
- 408 Fujian.

409

410

References

- 411 1. Novoselov, K. S.; Geim, A. K.; Morozov, S. V.; Jiang, D.; Zhang, Y.; Dubonos, S. V.; Grigorieva, I.
- V.; Firsov, A. A., Electric Field Effect in Atomically Thin Carbon Films. Science 2004, 306 (5696), 666-
- 413 669, DOI: 10.1126/science.1102896.
- 2. Nair, R. R.; Sepioni, M.; Tsai, I. L.; Lehtinen, O.; Keinonen, J.; Krasheninnikov, A. V.; Thomson,
- 415 T.; Geim, A. K.; Grigorieva, I. V., Spin-half paramagnetism in graphene induced by point defects. *Nat.*
- 416 *Phys.* **2012**, *8* (3), 199-202, DOI: 10.1038/nphys2183.
- 417 3. Fan, X.; Zhang, G.; Zhang, F., Multiple roles of graphene in heterogeneous catalysis. Chem. Soc.
- 418 Rev. **2015**, 44 (10), 3023-3035, DOI: 10.1039/C5CS00094G.
- 4.9 Park, J.; Yan, M., Covalent Functionalization of Graphene with Reactive Intermediates. Acc. Chem.
- 420 Res. **2013**, 46 (1), 181-189, DOI: 10.1021/ar300172h.
- 5. Liao, L.; Peng, H.; Liu, Z., Chemistry Makes Graphene beyond Graphene. J. Am. Chem. Soc. 2014,
- 422 *136* (35), 12194-12200, DOI: 10.1021/ja5048297.
- 6. Primo, A.; Neatu, F.; Florea, M.; Parvulescu, V.; Garcia, H., Graphenes in the absence of metals as
- 424 carbocatalysts for selective acetylene hydrogenation and alkene hydrogenation. Nat. Commun. 2014, 5
- 425 (1), 5291, DOI: 10.1038/ncomms6291.
- 426 7. Li, M.; Zhang, L.; Xu, Q.; Niu, J.; Xia, Z., N-doped graphene as catalysts for oxygen reduction and
- 427 oxygen evolution reactions: Theoretical considerations. J. Catal. 2014, 314, 66-72, DOI:
- 428 10.1016/j.jcat.2014.03.011.
- 429 8. Duan, X.; O'Donnell, K.; Sun, H.; Wang, Y.; Wang, S., Sulfur and Nitrogen Co-Doped Graphene

- 430 for Metal-Free Catalytic Oxidation Reactions. Small 2015, 11 (25), 3036-3044, DOI:
- 431 10.1002/smll.201403715.
- 432 9. Ma, Y.; Zhang, S.; Chang, C.-R.; Huang, Z.-Q.; Ho, J. C.; Qu, Y., Semi-solid and solid frustrated
- 433 Lewis pair catalysts. Chem. Soc. Rev. 2018, 47 (15), 5541-5553, DOI: 10.1039/C7CS00691H.
- 434 10. Stephan, D. W., The broadening reach of frustrated Lewis pair chemistry. *Science* **2016**, *354* (6317),
- 435 aaf7229, DOI: doi:10.1126/science.aaf7229.
- 436 11. Fontaine, F.-G.; Stephan, D. W., On the concept of frustrated Lewis pairs. *Philos. Trans. R. Soc.*, A
- 437 **2017,** *375* (2101), 20170004, DOI: 10.1098/rsta.2017.0004.
- 438 12. Wan, Q.; Lin, S.; Guo, H., Frustrated Lewis Pairs in Heterogeneous Catalysis: Theoretical Insights.
- 439 *Molecules* **2022**, *27* (12), 3734, DOI: 10.3390/molecules27123734.
- 13. Stephan, D. W., Frustrated Lewis Pairs: From Concept to Catalysis. Acc. Chem. Res. 2015, 48 (2),
- 441 306-316, DOI: 10.1021/ar500375j.
- 14. Riley, C.; Zhou, S.; Kunwar, D.; De La Riva, A.; Peterson, E.; Payne, R.; Gao, L.; Lin, S.; Guo, H.;
- Datye, A., Design of Effective Catalysts for Selective Alkyne Hydrogenation by Doping of Ceria with a
- Single-Atom Promotor. J. Am. Chem. Soc. **2018**, 140 (40), 12964-12973, DOI: 10.1021/jacs.8b07789.
- 445 15. Zhao, J.; Liu, X.; Chen, Z., Frustrated Lewis Pair Catalysts in Two Dimensions: B/Al-Doped
- 446 Phosphorenes as Promising Catalysts for Hydrogenation of Small Unsaturated Molecules. ACS Catal.
- **2017,** *7* (1), 766-771, DOI: 10.1021/acscatal.6b02727.
- 448 16. Liu, W.; Chen, Y.; Qi, H.; Zhang, L.; Yan, W.; Liu, X.; Yang, X.; Miao, S.; Wang, W.; Liu, C.; Wang,
- 449 A.; Li, J.; Zhang, T., A Durable Nickel Single-Atom Catalyst for Hydrogenation Reactions and Cellulose
- 450 Valorization under Harsh Conditions. Angew. Chem. Int. Ed. 2018, 57 (24), 7071-7075, DOI:
- 451 10.1002/anie.201802231.
- 452 17. Huang, Z.-Q.; Zhang, T.; Chang, C.-R.; Li, J., Dynamic Frustrated Lewis Pairs on Ceria for Direct
- 453 Nonoxidative Coupling of Methane. ACS Catal. **2019**, 9 (6), 5523-5536, DOI: 10.1021/acscatal.9b00838.
- 454 18. Ban, T.; Yu, X.-Y.; Kang, H.-Z.; Zhang, H.-X.; Gao, X.; Huang, Z.-Q.; Chang, C.-R., Design of
- 455 Single-Atom and Frustrated-Lewis-Pair Dual Active Sites for Direct Conversion of CH₄ and CO₂ to
- 456 Acetic Acid. J. Catal. 2022, 408, DOI: 10.1016/j.jcat.2022.03.004.
- 457 19. Yang, J.; Li, W.; Wang, D.; Li, Y., Single-Atom Materials: Small Structures Determine
- 458 Macroproperties. Small Struct. **2021**, *2* (2), 2000051, DOI: 10.1002/sstr.202000051.
- 459 20. Kauling, A. P.; Seefeldt, A. T.; Pisoni, D. P.; Pradeep, R. C.; Bentini, R.; Oliveira, R. V. B.;
- Novoselov, K. S.; Castro Neto, A. H., The Worldwide Graphene Flake Production. Adv. Mater. 2018, 30
- 461 (44), 1803784, DOI: 10.1002/adma.201803784.
- 462 21. Hegab, H. M.; ElMekawy, A.; Zou, L.; Mulcahy, D.; Saint, C. P.; Ginic-Markovic, M., The
- 463 controversial antibacterial activity of graphene-based materials. Carbon 2016, 105, 362-376, DOI:
- 464 10.1016/j.carbon.2016.04.046.
- 465 22. Mazánek, V.; Luxa, J.; Matějková, S.; Kučera, J.; Sedmidubský, D.; Pumera, M.; Sofer, Z.,
- 466 Ultrapure Graphene Is a Poor Electrocatalyst: Definitive Proof of the Key Role of Metallic Impurities in
- 467 Graphene-Based Electrocatalysis. ACS Nano 2019, 13 (2), 1574-1582, DOI: 10.1021/acsnano.8b07534.
- 468 23. Bøggild, P., The war on fake graphene. *Nature* **2018**, *562* (7728), 502-503, DOI: 10.1038/d41586-
- 469 018-06939-4.
- 470 24. Zhu, W.; Low, T.; Perebeinos, V.; Bol, A. A.; Zhu, Y.; Yan, H.; Tersoff, J.; Avouris, P., Structure and
- 471 Electronic Transport in Graphene Wrinkles. Nano Lett. 2012, 12 (7), 3431-3436, DOI:
- 472 10.1021/nl300563h.
- 473 25. Vicent, I. M.; Ochoa, H.; Guinea, F., Spin relaxation in corrugated graphene. Phys. Rev. B 2017, 95

- 474 (19), 195402, DOI: 10.1103/PhysRevB.95.195402.
- 475 26. Schultz, B.; Patridge, C.; Lee, V.; Jaye, C.; Lysaght, P.; Smith, C.; Barnett, J.; Fischer, D.;
- 476 Prendergast, D.; Banerjee, S., Imaging local electronic corrugations and doped regions in graphene. *Nat.*
- 477 *Commun.* **2011**, *2*, 372, DOI: 10.1038/ncomms1376.
- 478 27. McKay, H.; Wales, D. J.; Jenkins, S. J.; Verges, J. A.; de Andres, P. L., Hydrogen on graphene under
- 479 stress: Molecular dissociation and gap opening. Phys. Rev. B 2010, 81 (7), 075425, DOI:
- 480 10.1103/PhysRevB.81.075425.
- 481 28. Cui, L.; Du, X.; Wei, G.; Feng, Y., Thermal Conductivity of Graphene Wrinkles: A Molecular
- 482 Dynamics Simulation. J. Phys. Chem. C 2016, 120 (41), 23807-23812, DOI: 10.1021/acs.jpcc.6b07162.
- 483 29. Sun, R.-X.; Guo, Q.-Q.; Guo, H.-W.; Yan, X.-Q.; Liu, Z.-B.; Tian, J.-G., Photoresponse in a Strain-
- Induced Graphene Wrinkle Superlattice. J. Phys. Chem. Lett. 2020, 11 (13), 5059-5067, DOI:
- 485 10.1021/acs.jpclett.0c01535.
- 486 30. Deng, S.; Berry, V., Wrinkled, rippled and crumpled graphene: an overview of formation
- 487 mechanism, electronic properties, and applications. Mater. Today 2016, 19 (4), 197-212, DOI:
- 488 10.1016/j.mattod.2015.10.002.
- 489 31. Xu, K.; Cao, P.; Heath, J. R., Scanning Tunneling Microscopy Characterization of the Electrical
- Properties of Wrinkles in Exfoliated Graphene Monolayers. *Nano Lett.* **2009**, *9* (12), 4446-4451, DOI:
- 491 10.1021/nl902729p.
- 492 32. Kundalwal, S. I.; Meguid, S. A.; Weng, G. J., Strain gradient polarization in graphene. Carbon 2017,
- 493 117, 462-472, DOI: 10.1016/j.carbon.2017.03.013.
- 494 33. Duggen, L.; Willatzen, M.; Wang, Z. L., Mechanically Bent Graphene as an Effective Piezoelectric
- 495 Nanogenerator. J. Phys. Chem. C 2018, 122 (36), 20581-20588, DOI: 10.1021/acs.jpcc.8b05246.
- 496 34. Huang, X.; Zhao, W.; Zhu, C.; Chen, X.; Han, X.; Xing, J.; Bao, L.; Meng, L.; Shi, N. N.; Gao, P.;
- Liu, L.; Zhou, X.; Xu, F.; Ding, F.; Huang, Y., Modification of the Interlayer Coupling and Chemical
- 498 Reactivity of Multilayer Graphene through Wrinkle Engineering. Chem. Mater. 2021, 33 (7), 2506-2515,
- 499 DOI: 10.1021/acs.chemmater.0c04799.
- 500 35. Lui, C. H.; Liu, L.; Mak, K. F.; Flynn, G. W.; Heinz, T. F., Ultraflat graphene. Nature 2009, 462
- 501 (7271), 339-341, DOI: 10.1038/nature08569.
- 502 36. Kresse, G.; Furthmüller, J., Efficiency of ab-initio total energy calculations for metals and
- semiconductors using a plane-wave basis set. Comput. Mater. Sci. 1996, 6 (1), 15-50, DOI:
- 504 10.1016/0927-0256(96)00008-0.
- 505 37. Perdew, J. P.; Burke, K.; Ernzerhof, M., Generalized Gradient Approximation Made Simple. *Phys.*
- 506 Rev. Lett. 1996, 77 (18), 3865-3868, DOI: 10.1103/PhysRevLett.77.3865.
- 38. Perdew, J. P.; Wang, Y., Accurate and simple analytic representation of the electron-gas correlation
- 508 energy. Phys. Rev. B 1992, 45 (23), 13244-13249, DOI: 10.1103/PhysRevB.45.13244.
- 39. Blöchl, P. E., Projector augmented-wave method. *Phys. Rev. B* **1994**, *50* (24), 17953-17979, DOI:
- 510 10.1103/PhysRevB.50.17953.
- 511 40. Grimme, S., Semiempirical GGA-type density functional constructed with a long-range dispersion
- 512 correction. J. Comput. Chem. **2006**, 27 (15), 1787-1799, DOI: 10.1002/jcc.20495.
- 513 41. Tang, W.; Sanville, E.; Henkelman, G., A grid-based Bader analysis algorithm without lattice bias.
- 514 J. Phys.: Condens. Matter 2009, 21 (8), 084204, DOI: 10.1088/0953-8984/21/8/084204.
- 515 42. Sheppard, D.; Xiao, P.; Chemelewski, W.; Johnson, D. D.; Henkelman, G., A generalized solid-state
- 516 nudged elastic band method. J. Chem. Phys. 2012, 136 (7), 074103, DOI: 10.1063/1.3684549.
- 517 43. Xiao, P.; Sheppard, D.; Rogal, J.; Henkelman, G., Solid-state dimer method for calculating solid-

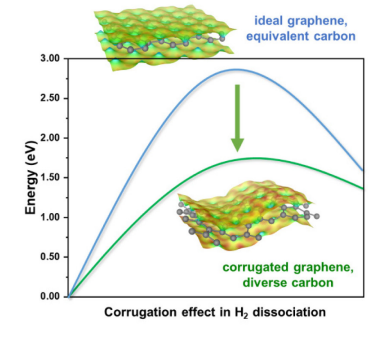
- 518 solid phase transitions. J. Chem. Phys. **2014**, 140 (17), 174104, DOI: 10.1063/1.4873437.
- 519 44. Jarzynski, C., Nonequilibrium Equality for Free Energy Differences. Phys. Rev. Lett. 1997, 78 (14),
- 520 2690-2693, DOI: 10.1103/PhysRevLett.78.2690.
- 521 45. Yan, H.; Zhao, X.; Guo, N.; Lyu, Z.; Du, Y.; Xi, S.; Guo, R.; Chen, C.; Chen, Z.; Liu, W.; Yao, C.;
- 522 Li, J.; Pennycook, S. J.; Chen, W.; Su, C.; Zhang, C.; Lu, J., Atomic engineering of high-density isolated
- 523 Co atoms on graphene with proximal-atom controlled reaction selectivity. Nat. Commun. 2018, 9 (1),
- 524 3197, DOI: 10.1038/s41467-018-05754-9.
- 525 46. Zhao, L.; He, R.; Rim Kwang, T.; Schiros, T.; Kim Keun, S.; Zhou, H.; Gutiérrez, C.; Chockalingam,
- 526 S. P.; Arguello Carlos, J.; Pálová, L.; Nordlund, D.; Hybertsen Mark, S.; Reichman David, R.; Heinz
- 527 Tony, F.; Kim, P.; Pinczuk, A.; Flynn George, W.; Pasupathy Abhay, N., Visualizing Individual Nitrogen
- 528 Dopants in Monolayer Graphene. Science **2011**, 333 (6045), 999-1003, DOI: 10.1126/science.1208759.
- 529 47. Preobrajenski, A. B.; Ng, M. L.; Vinogradov, A. S.; Mårtensson, N., Controlling graphene
- 530 corrugation on lattice-mismatched substrates. Phys. Rev. B 2008, 78 (7), 073401, DOI:
- 531 10.1103/PhysRevB.78.073401.
- 48. Banerjee, R.; Nguyen, V.-H.; Granzier-Nakajima, T.; Pabbi, L.; Lherbier, A.; Binion, A. R.; Charlier,
- J.-C.; Terrones, M.; Hudson, E. W., Strain Modulated Superlattices in Graphene. Nano Lett. 2020, 20 (5),
- 534 3113-3121, DOI: 10.1021/acs.nanolett.9b05108.
- 49. Hildebrand, M.; Abualnaja, F.; Makwana, Z.; Harrison, N. M., Strain Engineering of Adsorbate
- Self-Assembly on Graphene for Band Gap Tuning. J. Phys. Chem. C 2019, 123 (7), 4475-4482, DOI:
- 537 10.1021/acs.jpcc.8b09894.
- 538 50. Warner Jamie, H.; Margine Elena, R.; Mukai, M.; Robertson Alexander, W.; Giustino, F.; Kirkland
- Angus, I., Dislocation-Driven Deformations in Graphene. Science 2012, 337 (6091), 209-212, DOI:
- 540 10.1126/science.1217529.
- 51. Woo, T. K.; Margl, P. M.; Blöchl, P. E.; Ziegler, T., A Combined Car-Parrinello QM/MM
- 542 Implementation for ab Initio Molecular Dynamics Simulations of Extended Systems: Application to
- 543 Transition Metal Catalysis. J. Phys. Chem. B **1997**, 101 (40), 7877-7880, DOI: 10.1021/jp9717296.

545

546547

548

For Table of Contents Only



549